

Memorization and Generalization in Generative Diffusion under the Manifold Hypothesis

Beatrice Achilli^{*1}, Luca Ambrogioni^{†2}, Carlo Lucibello^{‡1}, Marc Mézard^{§1}, and Enrico Ventura^{¶1}

¹*Bocconi University*

²*Radboud University*

Abstract

We study the memorization and generalization capabilities of a Diffusion Model (DM) in the case of structured data defined on a latent manifold. We specifically consider a set of P mono-modal data points in N dimensions lying on a latent subspace of dimension $D = \alpha_D N$, according to the Hidden Manifold Model (HMM). Our analysis leverages the recently introduced formalism based on the statistical physics of the Random Energy Model (REM). We provide evidence for the existence of an onset time $t_o > t_c$ when traps appear in the potential without affecting the typical diffusive trajectory. The size of the basins of attraction of such traps is computed as a function of time. Moreover, we derive the collapse time t_c at which trajectories fall in the basin of one of the training points, implying memorization. An explicit formula for t_c is given as a function of P and the ratio α_D , proving that the curse of dimensionality issue does not hold for highly structured data, i.e. $\alpha_D \ll 1$, regardless of the non-linearity of the manifold surface. We also prove that collapse coincides with the condensation transition in the REM. Eventually, the degree of generalization of DMs is formulated in terms of the Kullback-Leibler divergence between the exact and the empirical distribution of the sampled configurations: we show the existence of an additional time $t_g < t_c < t_o$ such that the distance between the empirical measure of the data and the ground-truth is minimal. Counter-intuitively, the best generalization performance is found within the memorization phase of the model. We conclude that the generalization performance of DMs benefit from highly structured data since t_g approaches zero faster than t_c when $\alpha_D \rightarrow 0$.

1 Introduction

Generative diffusion models [30] reached the state-of-the-art performance on image generation [17, 31], sound [9] and video generation [18] by synthesizing data through a stochastic dynamical denoising process based on stochastic differential equations [31]. Recent work has established deep connections between the framework of generative diffusion and well-known phenomena in statistical physics [7, 25, 24, 2]. As an example, it was shown that class separation during the generative dynamics of diffusion models can be described in terms of symmetry breaking phase transitions [28, 8], which are the result of a Curie-Weiss self-consistency condition implicit in the fixed-point structure of the score function [2]. The presence of hierarchically organized and semantically

^{*}beatrice.achilli@unibocconi.it

[†]luca.ambrogioni@donders.ru.nl

[‡]carlo.lucibello@unibocconi.it

[§]marc.mezard@unibocconi.it

[¶]enrico.ventura@unibocconi.it

meaningful phase transitions was also demonstrated in [29]. Furthermore, it was recently discovered that the generative dynamics of diffusion models is closely related to the retrieval dynamics of continuous modern Hopfield networks [3, 19], which are a class of associative memory models with exponential theoretical capacity [21, 12, 20, 27]. By exploiting this connection, [8] used random energy techniques to characterize the memorization phenomenon in diffusion models in a way that mirrors the study of memory capacity of Hopfield models [23]. These techniques were also used in [1] to characterize the closure of gaps in the spectrum of the Jacobian of the score corresponding to *geometric memorization* effects, where sub-spaces of the target distributions are lost due to fine sample size.

In this paper, we provide a detailed theoretical analysis of generative diffusion models when the data is sampled from a low-dimensional, possibly non-linear, manifold using random energy and replica techniques. The paper is organized as follows:

- In Section 2 we introduce the Random Energy Model (REM) formalism that will be used along the entire analysis of the Diffusion Model (DM).
- In Sections 3 and 4, we apply the REM formalism in the context of DMs. When using the empirical score function as an approximation of the true one, we highlight the presence of two dynamical phase transitions when simulating the reverse process with time t going from $+\infty$ to 0.
 1. The first one, at time t_o , is called the onset transition. It is when basins of attraction arise in correspondence of most datapoints, but they are not large enough to affect typical trajectories.
 2. The second, at time $t_c < t_o$, is called collapse transition [8]. It corresponds to typical diffused particles being trapped in the potential well of one of the datapoints, with no chance of escaping it for the rest of the evolution. These last results are consistent with the very recent work [13].

For generically distributed datapoints, we show that the collapse transition corresponds to the condensation transition in the REM. Moreover, we show that for $t > t_c$ the empirical score is close to the true score.

- Eventually, in Section 5 we analyze the problem of generalization in DMs driven by the empirical score, using two approaches. We first compute the optimal stopping time t_g which is the time at which the KL divergence between the diffused empirical distribution and the target distribution is minimal. We use the REM formalism again to compute this stopping time t_g . We find that it is always located in the condensed phase, i.e. $t_g < t_c$, a phenomenon that has been observed recently in the related framework of kernel approximations to large dimensional densities [6]. In a second approach, we combine results obtained via REM formalism with random matrix computations (as performed in [32]), in order to deduce an empirical generalization criterion for generative diffusion before memorization.

2 The Random Energy Model formalism

In order to compute the main quantities that characterize Diffusion Models (DMs), we introduce the tools needed to solve a generic REM, following [23].

Let us consider $P = e^{\alpha N}$ (or equivalently $P = e^{\alpha N} - 1$) i.i.d. energy levels $\varepsilon^\mu \sim p(\varepsilon | \omega)$, where we extend the typical REM setting allowing for a common source of quenched disorder $\omega \sim p_\omega$. The goal is to compute the

average asymptotic free energy of the system, defined by

$$\phi_\alpha(\lambda) = \lim_{N \rightarrow \infty} \frac{1}{\lambda N} \mathbb{E} \log \sum_{\mu} e^{\lambda N \varepsilon^\mu} \quad (1)$$

It turns out that $\phi_\alpha(\lambda)$ can be simply expressed in terms of the cumulant generating function and its Legendre transform:

$$\zeta(\lambda) = \lim_{N \rightarrow \infty} \frac{1}{N} \mathbb{E}_\omega \log \mathbb{E}_{\varepsilon|\omega} e^{\lambda N \varepsilon}, \quad (2)$$

$$s(\varepsilon) = \sup_{\lambda} \varepsilon \lambda - \zeta(\lambda). \quad (3)$$

The total entropy of the system is $\Sigma(\varepsilon) = \alpha - s(\varepsilon)$. Let us define the quantities $\varepsilon_*(\alpha)$ and $\lambda_*(\alpha)$ respectively as the maximum value of the energy levels in the uncondensed phase, obtained as the largest root of $\Sigma(\varepsilon_*) = 0$, and the condensation threshold. In the uncondensed phase, i.e. when $\lambda < \lambda_*(\alpha)$, the dominating energy level $\tilde{\varepsilon}(\lambda)$ is obtained as the stationary point of $\lambda \varepsilon - s(\varepsilon)$, and by the Legendre transform definition of $\zeta(\lambda)$ this is equivalent to $\tilde{\varepsilon}(\lambda) = \zeta'(\lambda)$. The entropy of the dominating state can be rewritten as $\Sigma(\tilde{\varepsilon}(\lambda)) = \alpha - s(\tilde{\varepsilon}(\lambda)) = \alpha + \zeta(\lambda) - \lambda \zeta'(\lambda)$, so the condensation threshold $\lambda_*(\alpha)$ is obtained from the condensation condition

$$\alpha + \zeta(\lambda_*) - \lambda_* \zeta'(\lambda_*) = 0. \quad (4)$$

Finally, the free energy is given by

$$\phi_\alpha(\lambda) = \begin{cases} \frac{\alpha + \zeta(\lambda)}{\lambda} & \lambda < \lambda_*(\alpha), \\ \varepsilon_*(\alpha) & \lambda \geq \lambda_*(\alpha). \end{cases} \quad (5)$$

3 Diffusion Models

Diffusion Models (DMs) are physics-based state-of-the-art generative devices. These models are capable of generating new examples (e.g. images, videos) through a stochastic dynamical denoising process, occurring in time. Previous works in literature show that data features are progressively learned by DMs during a noising process, which is then reflected in the way the sample, during the de-noising procedure. The REM formalism is a powerful tool to explain such phenomenology, as showed by [8]. After introducing the physics DMs, we are going to tackle the context of highly structured data, specifically focusing on two - apparently complementary - aspects of the model performance:

- **Memorization:** the predisposition of the model to collapse onto the training-data in the last stage of the denoising process. We study how the tendency of these models to memorize change when data live on a latent manifold of a given dimension.
- **Generalization:** the capability of the model to learn the ground-truth distribution of the training-data. We implement the same techniques employed to study memorization to compute the optimal amount of denoising that is necessary to fit the data.

3.1 Modeling the Manifold Hypothesis

In this paper we focus on data points generated by a Hidden Manifold Model (HMM). The HMM is a simple synthetic generative process displaying the idea of the data manifold hypothesis [5], where data lie on D -dimensional submanifold of the ambient N -dimensional space. This generative process has been introduced and investigated in [15, 16, 14]. data points $\{\xi^\mu \in \mathbb{R}^N\}_{\mu=1}^P$ are generated as $\xi^\mu = \sigma\left(\frac{1}{\sqrt{D}}Fz^\mu\right)$, where the latent variables z^μ are Gaussian, $z^\mu \sim \mathcal{N}(0, I_D)$, σ is an element-wise non-linearity, and $F \in \mathbb{R}^{N \times D}$ is a random matrix with i.i.d. standard Gaussian entries. The number of data points is $P = e^{\alpha N}$, with α control parameter of the model. We define $\alpha_D = D/N$, and assume $D, N \rightarrow +\infty$ with α_D having a finite limit.

3.2 The model

Let us consider a forward diffusion process where starting from $x_{t=0} \sim p_0$ points evolve through the equation

$$dx_t = dW_t \quad (6)$$

where W_t is a Wiener process in N dimensions and $x_t \in \mathbb{R}^N$. Time by time x_t satisfies the probability distribution defined as p_t . This prescription for the forward process is known as *variance exploding*, in contrast to the *variance preserving* type of diffusion that has been also employed for analytical purposes [8, 11, 13, 4].

In the second phase, we start from Gaussian variable $x_{t=T} \sim \mathcal{N}(0, I_N \cdot \sqrt{T})$, and let it evolve through the backward process defined by

$$dx_t = -\nabla_x \log p_t(x)dt + dW_t \quad (7)$$

which takes time backward from $t_f = T \gg 1$ to $t = 0$. The term $S(x, t) = \nabla_x \log p_t(x)$ is called score function.

As for the data generating process, in the following we will focus on vectors coming from the HMM described in the previous section.

3.2.1 The True Score Function

Usually, the true data distribution is not known. In our synthetic setting, though, it can be explicitly written as

$$p_0(x) = \int Dz \delta\left(x - \sigma\left(\frac{Fz}{\sqrt{D}}\right)\right), \quad (8)$$

where Dz is the standard Gaussian measure in D dimensions, with zero mean and unit variance. Therefore, the density of the process at a given time t takes the form

$$p_t(x) = \int Dz \frac{1}{\sqrt{2\pi t}^N} e^{-\frac{1}{2t}\|x - \sigma\left(\frac{Fz}{\sqrt{D}}\right)\|^2}. \quad (9)$$

The score function can be obtained exactly from this expression in the case of linear activation, as shown in [32].

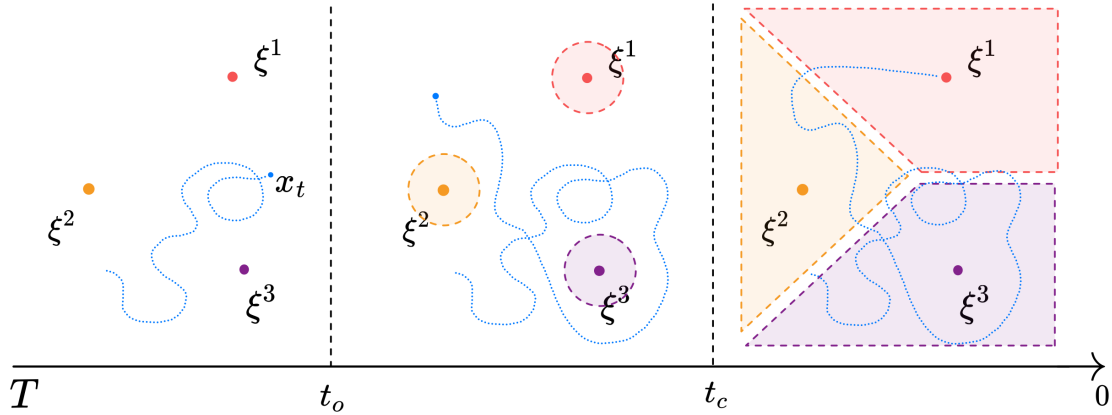


Figure 1: Pictorial representation of the phases identified in the backward process through the empirical score.

3.2.2 The Empirical Score Function

If we consider the empirical score function, the starting measure is $p_{0,\mathcal{D}}^{emp}(x) = \frac{1}{P} \sum_{\mu=1}^P \delta(x - \xi^\mu)$. After time t , the forward process generates points distributed according to the probability $p_t(x)$, whose empirical approximation is

$$p_{t,\mathcal{D}}^{emp}(x) = \frac{1}{P\sqrt{2\pi t}^N} \sum_{\mu=1}^P e^{-\frac{1}{2t}\|x - \xi^\mu\|^2}. \quad (10)$$

4 Memorization in Generative Diffusion

We here analyze the memorization phenomenology in generative diffusion when the model is trained on structured data. We will hereby use three expressions that all refer to the same dynamic process: *collapse*, *condensation* and *memorization*. The first two idioms, which derive from the REM terminology, will be proved to coincide in this framework, due to the typicality of the stochastic trajectories involved (see [1] for a case where this equivalence does not hold); the third concept, i.e. memorization, is more widely employed in the literature and we will use it as an umbrella term for the first two. Following [8], we are treating the attraction of the diffusive trajectories by the data points in terms of the collapse phase-transition occurring in an effective REM. We find two main dynamical events occurring in time:

1. The appearance of attractors with finite basins of attraction in the diffusion at time $t = t_o$. We call this time onset time, and it consists in the moment when training data become attractive, yet without influencing the typical diffusive trajectory of the model.
2. The collapse of the typical diffusive trajectory on the training data points, occurring at time $t = t_c < t_o$.

The mentioned phase separation is sketched in Fig. 1.

4.1 Collapse Time

Here we first recap the collapse condition for diffusion models as it was introduced in [8], and then proceed to compute it for our data generating model.

If we start the diffusion process from one of the data points, e.g. ξ^1 , then the typical trajectory is $x_t = \xi^1 + \omega\sqrt{t}$, with $\omega \sim \mathcal{N}(0, I)$. We want to see at which time t_c the term $\mu = 1$ dominates the summation in the measure, which for our choice of x_t takes the form

$$p_t^{emp}(x) = \frac{1}{P\sqrt{2\pi t}^N} \left(e^{-\frac{\|\omega\|^2}{2}} + \sum_{\mu \geq 2} e^{-\frac{1}{2t}\|(\xi^1 - \xi^\mu) + \omega\sqrt{t}\|^2} \right) \quad (11)$$

$$= \frac{1}{P\sqrt{2\pi t}} (Z_1 + Z_{2,\dots,P}). \quad (12)$$

In the limit of $P, N \rightarrow \infty$ with $\alpha = \frac{\log P}{N}$ fixed, we find $Z_1 \simeq e^{-N/2}$, while $\frac{1}{N} \log Z_{2,\dots,P}$ concentrates around ϕ_t , with

$$\phi_t = \frac{1}{N} \log \sum_{\mu \geq 2} e^{-\frac{1}{2t}\|(\xi^1 - \xi^\mu) + \omega\sqrt{t}\|^2}. \quad (13)$$

One can adopt a signal-to-noise type of reasoning, by comparing the concentrated versions of Z_1 and $Z_{2,\dots,P}$. This approach leads to the so-called *collapse* criterion, also used in [8, 23]. This criterion translates into requiring

$$\alpha + \zeta_{t_c}(1) = -\frac{1}{2}. \quad (14)$$

Since now the noise in the process is played by the factor λ/t , we are considering $\lambda^* = 1$. For given ξ^1 , ϕ_t is minus the free energy density of a REM, $\phi_t = \frac{1}{N} \log \sum_{\mu \geq 2} e^{\epsilon_\mu}$, with $P - 1$ energy levels $\epsilon_\mu = -\frac{1}{2t}\|(\xi^1 - \xi^\mu) + \omega\sqrt{t}\|^2$.

We then need to find the cumulant generating function for the energy levels

$$\zeta_t(\lambda) = \lim_{N \rightarrow +\infty} \frac{1}{N} \log \mathbb{E}_\epsilon e^{\lambda \epsilon} \quad (15)$$

$$= \lim_{N \rightarrow +\infty} \frac{1}{N} \mathbb{E}_{\xi^1, \omega} \log \mathbb{E}_{\xi^2} e^{-\frac{\lambda}{2t}\|(\xi^1 - \xi^\mu) + \omega\sqrt{t}\|^2} \quad (16)$$

If we assume that the data points come from a linear manifold, $\xi^\mu = \frac{1}{\sqrt{D}} F z^\mu$, then Eq. (16) becomes

$$\zeta_t(\lambda) = \lim_{N \rightarrow \infty} \frac{1}{N} \mathbb{E}_{F, z^1, \omega} \log \mathbb{E}_{z^2} e^{-\frac{\lambda}{2t}\|(F z^2 - F z^1) + \omega\sqrt{t}\|^2} \quad (17)$$

In order to investigate the scaling, let us simplify and assume that D dimensions have variance $\sigma_i^2 = \sigma^2$ and $N - D$ have variance $\sigma_i^2 = 0$. We have

$$\zeta_t(\lambda) = -\frac{1}{2}\alpha_D \log\left(1 + \frac{\lambda}{t}\sigma^2\right) - \frac{\lambda}{2}\alpha_D \frac{t + \sigma^2}{t + \lambda\sigma^2} - \frac{\lambda}{2}(1 - \alpha_D) \quad (18)$$

We can find the collapse time from the condition in Eq. (14) whose solution is

$$t_c = \frac{\sigma^2 N/D}{e^{2\log P/D} - 1}. \quad (19)$$

The collapse time depends on the manifold dimension and the number of hidden points. The so-called "curse of dimensionality", i.e. the need for a number of training data points that scales exponentially in the visible dimension of the data-space [35, 10], has been mitigated by the fact that we have an effective dimensionality for the data.

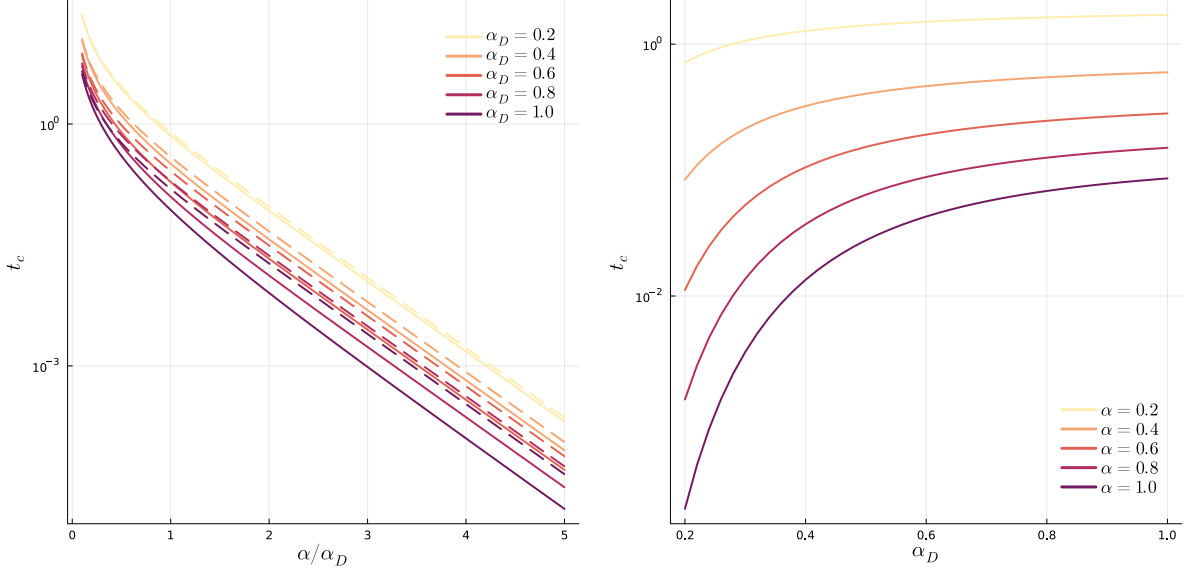


Figure 2: Semi-logarithmic plots of t_c in the linear manifold case (solid) compared to the Homogeneous Gaussian case (dashed) for different values of α_D (Left) and α (Right).

If we consider the limit of $D \ll \log P$ and $D \ll N$ we have

$$t_c \approx \frac{\sigma^2 N}{2 D} e^{-\frac{2 \log P}{D}} \quad (20)$$

which goes to zero fast.

In the general case where the data points come from a linear manifold, we can solve numerically the collapse equation derived in Appendix B.1. In Fig. 2 we show how t_c scales with the ratio α/α_D , i.e. $\log P/D$. These curves are compared with the Gaussian expression for t_c derived above. It is straightforward to notice that the slopes of the curves are the same for $\alpha \gg \alpha_D$, meaning that even in the linear manifold case we observe the same exponential scaling with $\log P/D$. What differs is the intercept, so the linear scaling with α_D is different (and non-linear). Fixing α , which here corresponds to fixing the number of data points, we see that the collapse time decreases with the hidden dimensionality D , and it happens earlier when we have less data points.

When we consider a non-linear manifold for the data points, $\xi^\mu = \sigma \left(\frac{1}{\sqrt{D}} F z^\mu \right)$, Eq. (16) takes the form

$$\zeta_t(\lambda) = \lim_{N \rightarrow +\infty} \frac{1}{N} \mathbb{E}_{z^1, F, \omega} \log \mathbb{E}_{z^2} e^{-\frac{\lambda}{2t} \left\| \left(\sigma \left(\frac{1}{\sqrt{D}} F z^1 \right) - \sigma \left(\frac{1}{\sqrt{D}} F z^2 \right) \right) + \omega \sqrt{t} \right\|^2}. \quad (21)$$

This can be computed using the replica method, as shown in Appendix B.2. We find an expression for ζ in the RS approximation

$$\zeta(q_d, q_0, m, \hat{q}_d, \hat{q}_0, \hat{m}) = -\alpha_D m \hat{m} - \frac{\alpha_D}{2} (q_d \hat{q}_d - q_0 \hat{q}_0) + \alpha_D G_S(\hat{q}_d, \hat{q}_0, \hat{m}) + G_E(q_d, q_0, m) \quad (22)$$

with

$$G_S(\hat{q}_d, \hat{q}_0, \hat{m}) = -\frac{1}{2} \log(1 - \hat{q}_d + \hat{q}_0) + \frac{1}{2} \frac{\hat{m}^2 + \hat{q}_0}{1 - \hat{q}_d + \hat{q}_0} \quad (23)$$

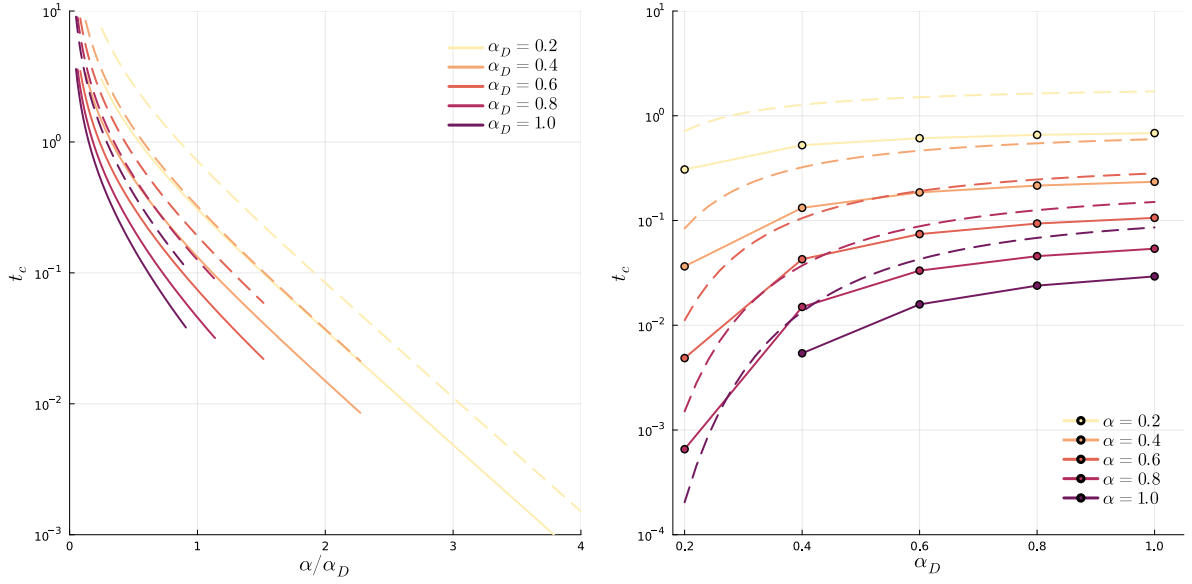


Figure 3: Semi-logarithmic plots of t_c in the hidden manifold case (solid) with tanh activation compared to the linear manifold case (dashed) for different values of α_D (Left) and α (Right).

and

$$G_E = \int D\omega \int D\gamma \int Du^0 \log \left(\int Du e^{-\frac{\lambda}{2t} (\sigma(u^0) - \sigma(\sqrt{q_d - q_0}u + mu^0 - \sqrt{q_0 - m^2}\gamma) + \sqrt{t}\omega)^2} \right). \quad (24)$$

Then we solve the saddle point equations (which depend on the choice of the non-linearity) to obtain the value of ζ at the fixed point. With this, we solve numerically the collapse condition, and the obtained scaling of the collapse time is compared to the one found for linear manifolds in Fig. 3.

4.1.1 Equivalence between Collapse and Condensation

In Eq. (14) we have introduced a criterion for collapse time. In Section 2 we have also discussed the condensation threshold for the REM which, in the context of DMs reads

$$\alpha + \zeta_{t_{cond}}(1) - \zeta'_{t_{cond}}(1) = 0. \quad (25)$$

In order to establish that the condensation and collapse phenomena happen at the same time, $t_c = t_{cond}$, we would therefore need to prove that

$$\zeta'_{t_c}(1) = -\frac{1}{2}. \quad (26)$$

This is indeed what we find for a typical trajectory as a consequence of the Nishimori condition. Computations are reported in Appendix C.

4.2 Onset Time and Basins of Attraction

We want to compute t_o , i.e. the time at which data points start to become attractors in the diffusion potential, although they do not influence the typical trajectories until t_c . This is the main difference with the *speciation* time computed by [7]: while the former is intrinsic in the data-set itself, the latter depends on the structure of the data points as divided in multiple classes and it does affect the direction of the diffusion in the ambient space.

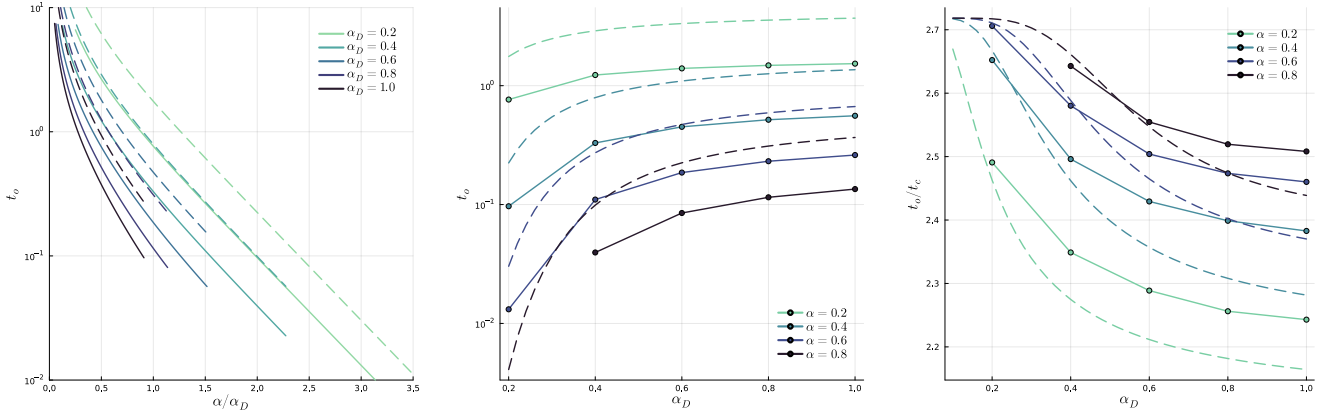


Figure 4: (Left) Onset time t_o as a function of α/α_D in semi-log scale for tanh activation; (Center) t_g as a function of α_D for fixed α in semi-log scale for tanh activation; (Right) comparison of the generalization time t_g with the collapse time t_c as a function of α_D when α is fixed and $\sigma = \tanh$.

The onset time can be computed setting $x_t = \xi^1$ and checking when $\phi = 0$. As done for the condensation time, let us compute it in the simple homogeneous Gaussian setting, where D variances are equal to σ^2 and the remaining ones are null. The moment-generating function of the relative REM is

$$\zeta_t(\lambda) = \lim_{N \rightarrow \infty} \frac{1}{N} \mathbb{E}_{\xi^1} \log \mathbb{E}_{\xi} e^{-\frac{\lambda}{2t} \|\xi^1 - \xi\|^2} = -\frac{\alpha_D}{2} \left(\log \left(1 + \frac{\lambda \sigma^2}{\alpha_D t} \right) + \frac{\lambda \sigma^2}{\alpha_D t + \lambda \sigma^2} \right). \quad (27)$$

In analogy with the collapse condition in Eq. (14), the on-set time condition must be

$$\zeta_{t_o}(1) + \alpha = 0, \quad (28)$$

which reads

$$\log \left(1 + \frac{\sigma^2}{\alpha_D t_o} \right) + \frac{\sigma^2}{\sigma^2 + \alpha_D t_o} - \frac{2\alpha}{\alpha_D} = 0. \quad (29)$$

The same calculation is then performed in the case of manifold structured data for different choices of the σ function. The computation is carried out by means of the replica method and it is reported in Appendix D. Results are reported in Fig. 4. The left panel in the figure shows the onset time as a function of the ratio α/α_D , suggesting that t_o behaves similarly to the condensation time t_c . The right panel shows how t_o/t_c increases when the data are more structured (i.e. when α_D decreases). Surprisingly, this quantity also reaches a constant value when α is fixed and $\alpha_D \rightarrow 0$. This particular behaviour of the onset time might be attributable to the exponentially large size of the basins of attraction of the data points.

Let us now consider a more general case where $x_t = \xi^1 + \omega \sqrt{R}$ where $\omega \sim \mathcal{N}(0, 1)$ and R is an arbitrary positive real value. Then one can repeat the calculation for the homogeneous Gaussian framework and obtain

$$\begin{aligned} \zeta_{t,R}(\lambda) &= \lim_{N \rightarrow \infty} \frac{1}{N} \mathbb{E}_{\xi^1, \omega} \log \mathbb{E}_{\xi} e^{-\frac{\lambda}{2t} \|(\xi^1 - \xi) + \omega \sqrt{R}\|^2} \\ &= -\frac{1}{2} \left(\alpha_D \log \left(1 + \frac{\lambda \sigma^2}{\alpha_D t} \right) + \frac{\alpha_D \lambda \sigma^2}{t} \frac{(t - \lambda R)}{\alpha_D t + \lambda \sigma^2} + \frac{\lambda R}{t} \right). \end{aligned} \quad (30)$$

$$= -\frac{1}{2} \left(\alpha_D \log \left(1 + \frac{\lambda \sigma^2}{\alpha_D t} \right) + \frac{\alpha_D \lambda \sigma^2}{t} \frac{(t - \lambda R)}{\alpha_D t + \lambda \sigma^2} + \frac{\lambda R}{t} \right). \quad (31)$$

Note that this expression for ζ coincides with Eq. (18) when $R = t$ and with Eq. (30) when $R = 0$. The new collapse

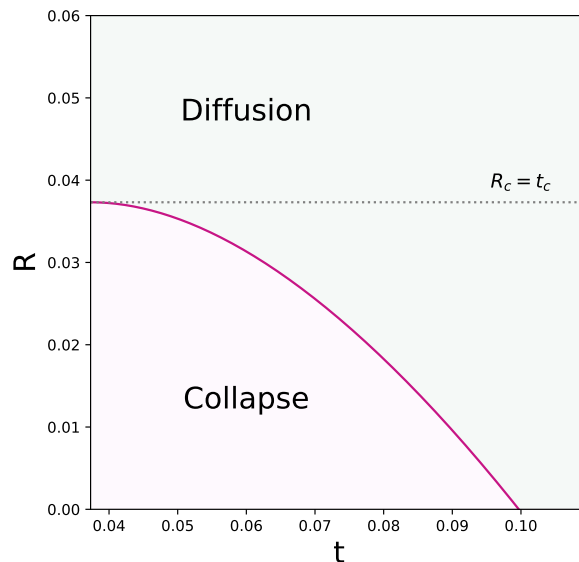


Figure 5: The value of R such that collapse onto the pattern is observed is indicated by the violet line, the violet area indicates the collapse region, while the particle diffuses in the green one. The radius becomes non-zero in $t = t_o$ and it equals the diffusion noise at $t = t_c$. Control parameters are chosen to be $\sigma^2 = 1, \alpha = 1, \alpha_D = 0.5$.

condition for $R(t)$ is given by

$$\zeta_{t, R_c}(1) + \alpha = -\frac{R_c}{2t}. \quad (32)$$

The value of R_c when $t \in [t_c, t_o]$ represents the main distance at which particles would start feeling the attraction to the pattern ξ^1 , i.e. the particle is in the basin of attraction of the pattern if $R < R_c$. Fig. 5 (Right) reports the size of the basins of attraction as a function of the time for one realization of $\sigma^2, \alpha, \alpha_D$. The radius R starts assuming non-zero values at $t = t_o$ and equals the noise of stochastic process $R_c = t_c$ when $t = t_c$. When $t \in [0, t_c]$ each possible trajectory (both typical and non-typical) has collapsed in one of the basins, by definition of collapse in the REM.

5 Generalization in Generative Diffusion

In this Section we compute the optimal time t_g such that the empirical probability distribution of a DM better fits the target distribution. The degree of generalization of a DM driven by its empirical score can be quantified in terms of the Kullback-Leibler (KL) divergence between the empirical probability distribution of the model and the distribution of the data points on the manifold. We first show that the true score and the empirical one do not differ, in the large volume limit, above the collapse transition. Secondly, we calculate t_g for different choices of α and α_D , showing that this times is always contained within the condensed phase of the auxiliary REM, i.e. the memorization phase of the DM. A similar effect has been found when seeking the best kernel to approximate probability densities from large-dimensional data: the optimal kernel width is found in the condensed phase [6]. Eventually, since the computation of t_g relies on the presence of collapse over the training-set, which is not always encountered in real world applications of Generative Diffusion, we propose an alternative criterion to define generalization in DMs.

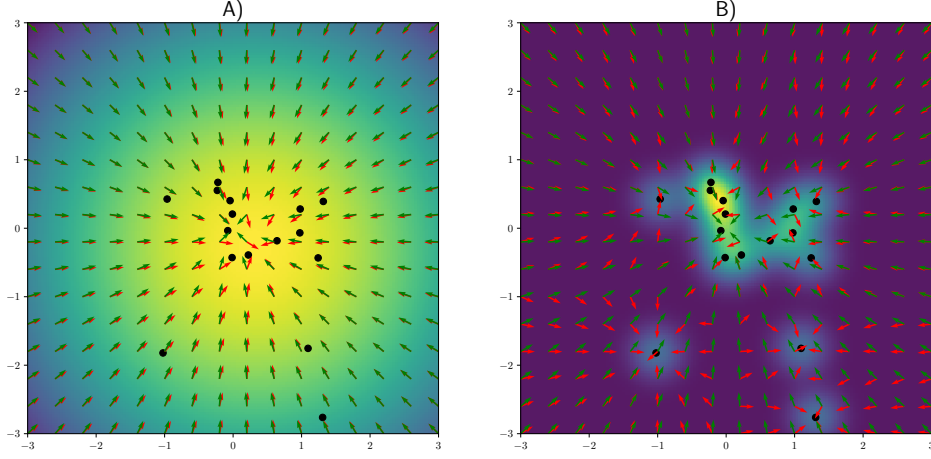


Figure 6: Visualization of the density, empirical score (red arrows) and exact score (green arrows) $t > t_c$ and $t < t_c$ (panels A and B respectively). The black dots denote individual data points. The score transitions from a phase where its direction is dominated by the expectation (i.e. the exact score) to a phase where its orientation is mostly determined by the individual data points (i.e. by the quenched fluctuations).

5.1 True vs Empirical Distribution

The Kullback-Leibler (KL) divergence between the true and empirical distribution is

$$\lim_{N \rightarrow \infty} \frac{1}{N} \mathbb{E}_{\mathcal{D}} D_{KL}[p_t(x) | p_{t,\mathcal{D}}^{emp}(x)] = \lim_{N \rightarrow \infty} \frac{1}{N} \mathbb{E}_{\mathcal{D}} \left[\int dx_t p_t(x) \log p_t(x) - \int dx p_t(x) \log p_{t,\mathcal{D}}^{emp}(x) \right] \quad (33)$$

In the uncondensed phase we can exploit the fact that the annealed approximation holds, combined with $\mathbb{E}_{\mathcal{D}} [p_{t,\mathcal{D}}^{emp}(x)] = p_t(x)$ to obtain

$$\lim_{N \rightarrow \infty} \frac{1}{N} \mathbb{E}_{\mathcal{D}} D_{KL}[p_t(x) | p_{t,\mathcal{D}}^{emp}(x)] = \begin{cases} 0 & \text{uncondensed phase} \\ \varepsilon^*(t, \alpha) - \alpha - \frac{1}{2} \log(2\pi t) - H_t & \text{condensed phase} \end{cases} \quad (34)$$

with $\varepsilon^*(t, \alpha) = -\lim_{N \rightarrow \infty} \mathbb{E}_{x,\mathcal{D}} \frac{1}{2Nt} \|x_t - \xi^*(x_t, \mathcal{D})\|^2$ and ξ^* being the nearest neighbor to x among the data points, while H_t is an additional time dependent term. The divergence between the empirical and true scores starting from t_c is represented in the bi-dimensional plot contained in Fig. 6 for one explanatory diffusion experiment, and it is validated by Fig. 7 relative to a further analysis of generalization.

5.2 Generalization Time: Generalizing while Collapsing

We would like to understand if there is a time at which the empirical score function points towards the original data manifold and not directly to the data points. To study this, we compute the KL divergence between the target distribution, i.e. p_0 , and the empirical distribution at time t , and then minimize to find the *generalization time*.

$$\lim_{N \rightarrow \infty} \frac{1}{N} \mathbb{E}_{\mathcal{D}} D_{KL}[p_0 | p_{t,\mathcal{D}}^{emp}] = \lim_{N \rightarrow \infty} \frac{1}{N} \mathbb{E}_{\mathcal{D}} \left[\int dx p_0(x) \log p_0(x) - \int dx p_0(x) \log p_{t,\mathcal{D}}^{emp}(x) \right]. \quad (35)$$

The second term can be computed using the REM formalism (see Appendix E) as

$$\tilde{D}_{KL}[p_0 | p_t^{emp}] = -\lim_{N \rightarrow \infty} \frac{1}{N} \mathbb{E}_{\mathcal{D}} \int dx p_0(x) \log p_{t,\mathcal{D}}^{emp}(x) \simeq -\phi_{t,\alpha}(1) + \alpha + \frac{1}{2} \log(2\pi t). \quad (36)$$

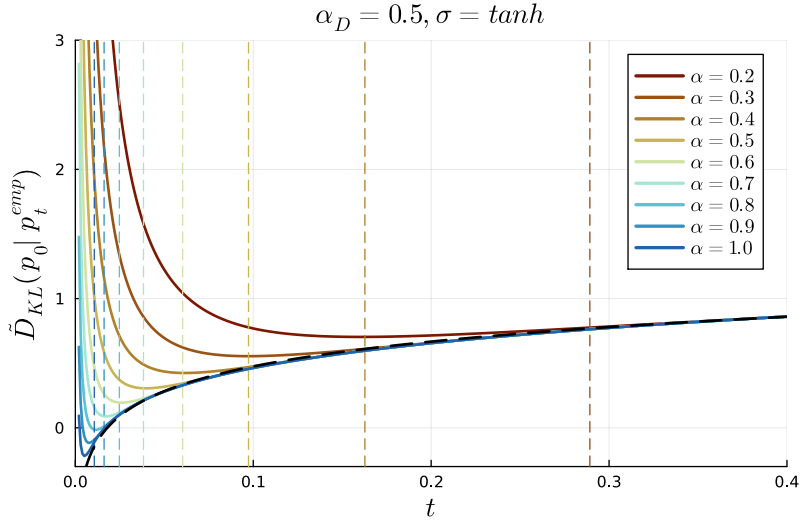


Figure 7: Time-dependent component of the KL divergence between target distribution and empirical distribution at time t for different values of α with \tanh activation. We report with colored dashed lines the condensation time t_c at the corresponding value of α , and with the black dashed line the limit $\alpha \rightarrow \infty$.

We show the behavior of the KL divergence for data from a hidden manifold model with \tanh non-linearity in Fig. 7. Interestingly, the time t_g where the discrepancy between p_0 and p_t^{emp} reaches a minimum is always smaller than the corresponding collapse time (reported as a dashed line in the Figure): the best generalization of the DM is reached inside the condensation phase, while the diffusive trajectory is trapped into the basin of attraction of the closest data point. It is also worth to notice that

$$\lim_{\alpha \rightarrow \infty} \tilde{D}_{KL}[p_0 | p_t^{emp}] = \tilde{D}_{KL}[p_0 | p_t]$$

where $p_t(x)$ is the exact probability distribution of the diffusive process. This quantity is represented by the line onto which all the curves in Fig. 7 collapse, i.e. the black dashed line in the figure: the computation in Eq. (34) is validated by the fact that curves start diverging from the asymptotic line exactly at $t = t_c(\alpha)$. Moreover, Fig. 8 (Left) displays that t_g decreases with α_D when α is fixed, while Fig. 8 (Right) shows that the ratio t_g/t_c vanishes when $\alpha_D \rightarrow 0$. This result means that t_g goes to zero faster than the collapse time t_c . We can thus conclude that a high structure of the data helps the empirical-score-driven diffusion model for two reasons:

- Both t_c and t_g are pushed towards $t = 0$ when $\alpha_D \rightarrow 0$ but the generalization time is moving faster towards smaller times. Since t_g represents the best stopping time to sample along the backward process, the condensation threshold, i.e. t_c , becomes irrelevant for the sake of sampling.
- Since the generalization time occurs inside the memorization phase, i.e.

$$0 < t_g < t_c \quad \forall \alpha, \alpha_D,$$

and the Kullback-Leibler distance between p_0 and p_t^{emp} is a monotonic function in $t \in [t_g, t_c]$ i.e.

$$\tilde{D}_{KL}[p_0 | p_{t_c}^{emp}] > \tilde{D}_{KL}[p_0 | p_{t_g}^{emp}] > 0,$$

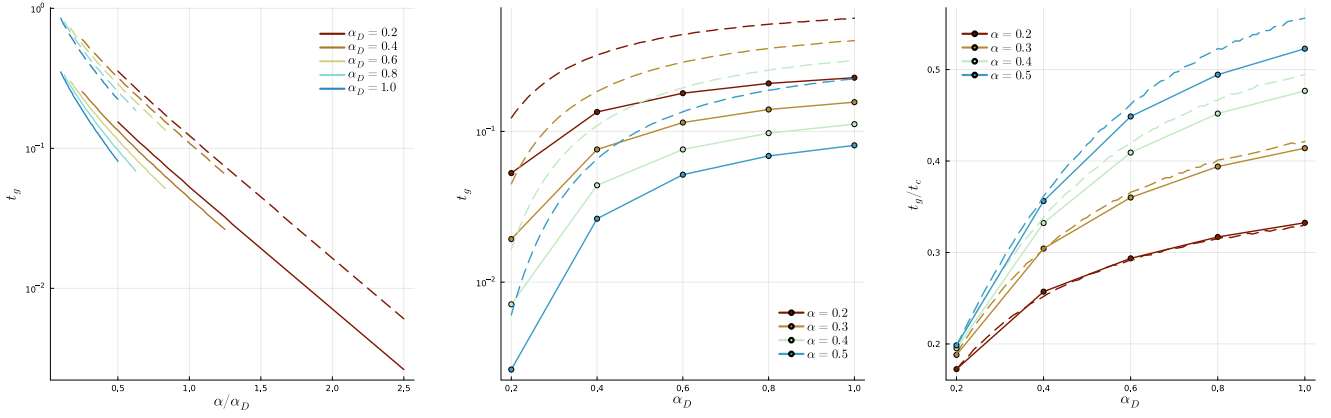


Figure 8: (Left) Generalization time t_g as a function of α/α_D in semi-log scale for tanh (solid) and linear (dashed) activation; (Center) t_g as a function of α_D for fixed α in semi-log scale for tanh (solid) and linear (dashed) activation; (Right) comparison of the generalization time t_g with the collapse time t_c as a function of α_D when α is fixed for tanh (solid) and linear (dashed) activation.

and the empirical model tends to the exact one when $\alpha_D \rightarrow 0$ i.e.

$$\lim_{\alpha_D \rightarrow 0} \lim_{N \rightarrow \infty} \frac{1}{N} \mathbb{E}_{\mathcal{D}} D_{KL}[p_0 | p_{t_c, \mathcal{D}}^{emp}] = 0,$$

then we must have

$$\lim_{\alpha_D \rightarrow 0} \lim_{N \rightarrow \infty} \frac{1}{N} \mathbb{E}_{\mathcal{D}} D_{KL}[p_0 | p_{t_g, \mathcal{D}}^{emp}] = 0$$

which means that the degree of generalization of the DM improves when data is more structured.

5.3 Generalization Condition: Generalizing before Collapsing

We now propose a more empirical definition of generalization for diffusion models. The main idea consists of sampling configurations from the data-manifold before the model condensates. The current definition of generalization is supported by the common routine used in generative modeling consisting in early-stopping the stochastic sampling process [22, 33, 34], with the aim of improving the quality of the examples. Consistently with [22], our analysis shows that we need a polynomial number of training data points to obtain generalization without falling into memorization.

Let us consider the exact score function measured from a data-set embedded in a linear manifold (see Section 3.2.1): we have proved in Section 5.1 that the true score coincides with the empirical one for $t > t_c$. The argument around the linear manifold can be extended to a non-linear one by observing that the interesting phenomenology in DMs occur at very small times (mainly due to the data structure, see Section 5), where the amplitude of the stochastic noise \sqrt{t} is much smaller than the manifold curvature. A more extensive dissertation about this aspect can be found in [32]. When F is a random matrix with i.i.d. standard Gaussian entries, $F^\top F/D$ is a Wishart matrix and its eigenvalues satisfy the Marchenko-Pastur distribution. As showed in [32], the Jacobian of the empirical score function before condensation is given by

$$J_t = \frac{1}{t} F \left[I_D + \frac{1}{t} F^\top F \right]^{-1} F^\top - I_N, \quad (37)$$

where we have re-absorbed the $1/D$ factor for the sake of clarity. Therefore, the spectrum of the eigenvalues of J_t can be derived by a propagation of the spectrum of $F^\top F$ and it is

$$\rho_t(r) = (1 - \alpha_m) \delta(r + 1) \theta[\alpha_D^{-1} - 1] - \frac{\alpha_D}{2\pi} \frac{1}{r(1+r)} \sqrt{(r_+ - r)(r - r_-)} \theta[(r_+ - r)(r - r_-)], \quad (38)$$

with $r_\pm(t) = -\frac{t}{(1 \pm \frac{1}{\sqrt{\alpha_D}})^2 + t}$. The first term in $\rho_t(r)$ is a spike in $r = -1$ with mass equal to $(1 - \alpha_D)$, the second term is a bulk of mass α_D , ranging in $[r_-(t), r_+(t)]$, and moving from $r = -1$ towards $r = 0$. Let us define $\Delta(t) = r_-(t) + 1$ as the width of the gap between $r = -1$ and $r = r_-(t)$. We know that $\lim_{t \rightarrow 0^+} \Delta(t) = 1$. We can hence find the approximate time at which the score function points towards the manifold t_g^{RMT} by imposing $\Delta(t_g^{RMT}) = \Delta$, with Δ that will be chosen to be small. This relation implies

$$t_g^{RMT}(\Delta) = \left(1 - \frac{1}{\sqrt{\alpha_D}}\right)^2 \left(\frac{1 - \Delta}{\Delta}\right). \quad (39)$$

Let us compute the condition such that the score is sufficiently orthogonal to the manifold (i.e. the model generates examples that live on the data-manifold) and it has not collapsed yet. Such condition reads

$$t_c \leq t_g^{RMT}(\Delta). \quad (40)$$

Let us assume to be in the $D \ll \log P$ and $D \ll N$ regime where t_c is given by Eq. (20). Moreover, we choose $\Delta = 1 - \epsilon$ with ϵ arbitrary small and positive. Hence, condition (40) reads

$$t_c \approx \frac{1}{2\alpha_D} e^{-\frac{2\alpha}{\alpha_D}} \leq \frac{1}{2} \left(1 - \frac{1}{\sqrt{\alpha_D}}\right)^2 \left(\frac{1 - \Delta}{\Delta}\right) \simeq \frac{\epsilon}{2\alpha_D}, \quad (41)$$

where we employed the fact that

$$\left(1 - \alpha_D^{-1/2}\right)^2 \simeq \alpha_D^{-1}, \quad (42)$$

when $\alpha_D \ll 1$. Eq. (41) thus becomes

$$e^{\frac{2\alpha}{\alpha_D}} \geq \epsilon^{-1}. \quad (43)$$

As a consequence, the minimum amount of data points such that the generalization condition (40) is satisfied, must scale as

$$P_{\min} = \epsilon^{-\frac{D}{2}}, \quad (44)$$

which is, yet again, a function of the dimension of the manifold rather than the ambient space.

6 Conclusions

In this paper we have extensively analyzed the memorization and generalization performance of a diffusion model (DM) that samples from a target distribution which is the empirical probability distribution of a set of data. Our main contribution, in this matter, is extending the Random Energy Model (REM) framework introduced by [8, 23] to the case of structured data living on a hidden manifold. Our study has allowed to understand the role of the manifold structure in learning the ground-truth distribution underneath the training set.

Firstly, we find that empirical-score-driven DMs can both memorize and generalize a set of data points at different times. We highlighted a rich sequence of dynamical phases occurring during the backward diffusion process that starts from $t = T$ and reaches $t = 0$:

- $t > t_o$: diffusive trajectories explore a convex diffusion potential. Sampling in this phase does not display any trait of generalization.
- $t_c < t \leq t_o$: diffusive trajectories explore a diffusion potential which is now multistable, since data points have become local minima surrounded by basins of attraction that grow while time decreases. The typical stochastic path of the system is not trapped into one of the basins, without showing any trace of memorization.
- $t_g \leq t \leq t_c$: the diffusive trajectory is now trapped into the basin of attraction and the empirical score function points towards the closest data point. At the same time the trajectory is also approaching the hidden data-manifold. The highest proximity between the empirical distribution of the states sampled by diffusion and the ground-truth distribution of the data points is reached at $t = t_g$. This time can be interpreted as the optimal stopping time for sampling.
- $0 < t < t_g$: the quality of the sampled examples now deteriorates until full memorization is reached at $t = 0$.

Note that the so-called *speciation time* studied in [8, 2], understood as the time when the diffusive potential undergoes a spontaneous symmetry breaking into multiple ergodic components that are representative of the data classes, has not been analyzed in our paper. Our study focuses in fact on DMs that learn mono-modal data points. We refer the reader to [13] for the study of the speciation time under the manifold hypothesis.

Surprisingly, the best degree of generalization is reached inside the memorization phase of the model, while the score function drives the model towards the closest attractor. The dynamical picture of the DM reported above is deformed by the presence of structure in the data, as it emerged from our analysis. Specifically, when α is fixed and $\alpha_D \rightarrow 0$:

1. Even though the onset time exponentially decreases, the distance between t_o and the condensation time increases until reaching a constant plateau.
2. The collapse time t_c shrinks towards $t = 0$, and the empirical-score-drive DM tends to the exact model, hence reducing the volume of the memorization phase of the model. This result is consistent with the very recent result obtained by [13] in the matter of variance-preserving DMs.
3. The generalization time t_g also moves towards $t = 0$, yet faster than t_c .

In light of point (3) we conclude that DMs benefit from highly structured data, even when α_D has not completely vanished, since the model can be basically stopped at $t \simeq 0$ and obtain a good degree of generalization, as one would obtain through a neural-network-trained model.

As an alternative to this definition of generalization, we use a combination of the REM formalism and Random Matrix Theory (RMT) to provide the reader with the minimal number of training data point to build the empirical score function in such a way that the DM is capable of sampling from the manifold without having entered the memorization phase. We find that the size of the data set needs to scale exponentially with the latent dimension of the data, instead of the visible dimension, mitigating the curse of dimensionality that affects learning in generative models [35, 10].

References

- [1] Beatrice Achilli, Enrico Ventura, Gianluigi Silvestri, Bao Pham, Gabriel Raya, Dmitry Krotov, Carlo Lucibello, and Luca Ambrogioni. Losing dimensions: Geometric memorization in generative diffusion. *arXiv:2410.08727*, 2024.
- [2] Luca Ambrogioni. The statistical thermodynamics of generative diffusion models: Phase transitions, symmetry breaking and critical instability, 2024. *arXiv:2310.17467*.
- [3] Luca Ambrogioni. In search of dispersed memories: Generative diffusion models are associative memory networks. *Entropy*, 5(26):381, 2024.
- [4] Santiago Aranguri, Giulio Biroli, Marc Mezard, and Eric Vanden-Eijnden. Optimizing noise schedules of generative models in high dimensions. *arXiv:2501.00988*, 2025.
- [5] Yoshua Bengio, Aaron Courville, and Pascal Vincent. Representation learning: A review and new perspectives. *IEEE Transactions on Pattern Analysis and Machine Intelligence*, 35(8):1798–1828, 2013.
- [6] Giulio Biroli and Marc Mézard. Kernel density estimators in large dimensions. *arXiv:2408.05807*, 2024.
- [7] Giulio Biroli and Marc Mézard. Generative diffusion in very large dimensions. *Journal of Statistical Mechanics: Theory and Experiment*, 2023(9):093402, 2023.
- [8] Giulio Biroli, Tony Bonnaire, Valentin de Bortoli, and Marc Mézard. Dynamical regimes of diffusion models. *Nature Communications*, 15(1):9957, 2024. ISSN 2041-1723.
- [9] Nanxin Chen, Yu Zhang, Heiga Zen, Ron J. Weiss, Mohammad Norouzi, and William Chan. Wavegrad: Estimating gradients for waveform generation, 2020. *arXiv:2009.00713*.
- [10] George Cybenko. Approximation by superpositions of a sigmoidal function. *Math. Control Signals Systems*, 2: 303–314, 1989.
- [11] Valentin De Bortoli. Convergence of denoising diffusion models under the manifold hypothesis, 2023. *arXiv:2208.05314*.
- [12] Mete Demircigil, Judith Heusel, Matthias Löwe, Sven Upgang, and Franck Vermet. On a model of associative memory with huge storage capacity. *Journal of Statistical Physics*, 168:288–299, 2017.
- [13] Anand Jerry George, Rodrigo Veiga, and Nicolas Macris. Analysis of diffusion models for manifold data. *arXiv:2502.04339*, 2025.
- [14] Federica Gerace, Bruno Loureiro, Florent Krzakala, Marc Mézard, and Lenka Zdeborová. Generalisation error in learning with random features and the hidden manifold model. In *International Conference on Machine Learning*, pages 3452–3462. PMLR, 2020.
- [15] Sebastian Goldt, Marc Mézard, Florent Krzakala, and Lenka Zdeborová. Modeling the influence of data structure on learning in neural networks: The hidden manifold model. *Physical Review X*, 10(4):041044, 2020.

- [16] Sebastian Goldt, Bruno Loureiro, Galen Reeves, Florent Krzakala, Marc Mézard, and Lenka Zdeborová. The gaussian equivalence of generative models for learning with shallow neural networks. In *Mathematical and Scientific Machine Learning*, pages 426–471. PMLR, 2022.
- [17] Jonathan Ho, Ajay Jain, and Pieter Abbeel. Denoising diffusion probabilistic models. In *Neural Information Processing Systems*. NeurIPS, 2020.
- [18] Jonathan Ho, Tim Salimans, Alexey Gritsenko, William Chan, Mohammad Norouzi, and David J. Fleet. Video diffusion models, 2022. arXiv:2204.03458.
- [19] Benjamin Hoover, Hendrik Strobelt, Dmitry Krotov, Judy Hoffman, Zsolt Kira, and Duen Horng Chau. Memory in Plain Sight: A Survey of the Uncanny Resemblances between Diffusion Models and Associative Memories, 2023. arXiv:2309.16750.
- [20] Dmitry Krotov. A new frontier for hopfield networks. *Nature Reviews Physics*, pages 1–2, 2023.
- [21] Dmitry Krotov and John Hopfield. Dense associative memory for pattern recognition. *Advances in Neural Information Processing Systems*, 2016.
- [22] Puheng Li, Zhong Li, Huishuai Zhang, and Jiang Bian. On the generalization properties of diffusion models. In A. Oh, T. Naumann, A. Globerson, K. Saenko, M. Hardt, and S. Levine, editors, *Advances in Neural Information Processing Systems*, volume 36, pages 2097–2127. Curran Associates, Inc., 2023.
- [23] Carlo Lucibello and Marc Mézard. The Exponential Capacity of Dense Associative Memories. *Physical Review Letters*, 132:077301, 2024.
- [24] Andrea Montanari. Sampling, Diffusions, and Stochastic Localization, 2023. arXiv:2305.10690.
- [25] Andrea Montanari and Yuchen Wu. Posterior Sampling from the Spiked Models via Diffusion Processes, 2023. arXiv:2304.11449.
- [26] Hidetoshi Nishimori. Exact results and critical properties of the ising model with competing interactions. *J. Phys. C: Solid State Phys.*, 13:4071–4076, 1980.
- [27] H. Ramsauer, B. Schäfl, J. Lehner, P. Seidl, M. Widrich, T. Adler, L. Gruber, M. Holzleitner, M. Pavlović, G. K. Sandve, et al. Hopfield networks is all you need. *International Conference on Learning Representations*, 2021.
- [28] Gabriel Raya and Luca Ambrogioni. Spontaneous symmetry breaking in generative diffusion models. In *Neural Information Processing Systems*. NeurIPS, 2023.
- [29] Antonio Sclocchi, Alessandro Favero, and Matthieu Wyart. A phase transition in diffusion models reveals the hierarchical nature of data, 2024. arXiv:2402.16991.
- [30] Jascha Sohl-Dickstein, Eric A. Weiss, Niru Maheswaranathan, and Surya Ganguli. Deep unsupervised learning using nonequilibrium thermodynamics. In *International Conference on Machine Learning*. ICML, 2015.
- [31] Yang Song, Jascha Sohl-Dickstein, Diederik P. Kingma, Abhishek Kumar, Stefano Ermon, and Ben Poole. Score-based generative modeling through stochastic differential equations. In *International Conference on Learning Representations*. ICLR, 2020.

- [32] Enrico Ventura, Beatrice Achilli, Gianluigi Silvestri, Carlo Lucibello, and Luca Ambrogioni. Manifolds, random matrices and spectral gaps: The geometric phases of generative diffusion, 2024. arXiv:2410.05898.
- [33] Hongkang Yang and Weinan E. Generalization error of gan from the discriminator’s perspective. *Research in the Mathematical Sciences*, 9, 2021.
- [34] Hongkang Yang and Weinan E. Generalization and memorization: The bias potential model. In Joan Bruna, Jan Hesthaven, and Lenka Zdeborova, editors, *Proceedings of the 2nd Mathematical and Scientific Machine Learning Conference*, volume 145 of *Proceedings of Machine Learning Research*, pages 1013–1043. PMLR, 2022.
- [35] Dmitry Yarotsky. Error bounds for approximations with deep relu networks. *Math. Control Signals Systems*, 94: 103–114, 2017.

A Collapse Time for Homogeneous Gaussian Data

When the data points live a linear manifold we can consider the basis in which the manifold has diagonal covariance matrix Σ with elements σ_i^2 (distributed according to the Marchenko-Pastur distribution).

In order to investigate the scaling, let's simplify and assume that D dimensions have variance $\sigma_i^2 = \sigma^2$ and $N - D$ have variance $\sigma_i^2 = 0$. We have

$$\zeta_t(\lambda) = -\frac{1}{2}\alpha_D \log\left(1 + \frac{\lambda}{\alpha_D t} \sigma^2\right) - \frac{\lambda}{2}\alpha_D \frac{t\alpha_D + \sigma^2}{t\alpha_D + \lambda\sigma^2} - \frac{\lambda}{2}(1 - \alpha_D) \quad (45)$$

We can find the collapse time from the condition

$$\zeta_{t_c}(1) + \alpha = -\frac{1}{2} \quad (46)$$

which implies

$$-\alpha_D \log\left(1 + \frac{\sigma^2}{\alpha_D t}\right) - 1 + 2\alpha = -1 \quad (47)$$

The solution is

$$t_c = \frac{\sigma^2 N/D}{e^{2 \log P/D} - 1}. \quad (48)$$

It results that the collapse time depends on the manifold dimension and the number of hidden points. If we consider the limit of $D \ll \log P$ and $D \ll N$ we have

$$t_c \approx \sigma^2 \frac{N}{D} e^{-\frac{2 \log P}{D}} \quad (49)$$

which goes to zero exponentially fast.

B Condensation Time: Computation of the Generating function

B.1 Linear case

In the variance exploding case we have

$$\zeta_t(\lambda) = \lim_{N \rightarrow \infty} \frac{1}{N} \mathbb{E}_{F, z^1, \omega} \log \mathbb{E}_{z^2} e^{-\frac{\lambda}{2t} \left\| \left(\frac{F}{\sqrt{D}} z^2 - \frac{F}{\sqrt{D}} z^1 \right) + \omega \sqrt{t} \right\|^2} \quad (50)$$

$$= \lim_{N \rightarrow \infty} \frac{1}{N} \mathbb{E}_{F, z^1, \omega} \log \int \frac{dz^2}{2\pi} e^{-\frac{1}{2} z^2 (I + \frac{\lambda}{t} \frac{F^T F}{D}) z^2 + \frac{\lambda}{t} z^2 \left(\frac{F^T F}{D} z^1 - \frac{F^T}{\sqrt{D}} \omega \sqrt{t} \right) - \frac{\lambda}{2t} \left\| -\frac{F}{\sqrt{D}} z^1 + \omega \sqrt{t} \right\|^2} \quad (51)$$

$$(52)$$

$$\begin{aligned}
&= \lim_{N \rightarrow \infty} \frac{1}{N} \mathbb{E}_{F, z^1, \omega} \left[-\frac{1}{2} \log \det \left(I + \frac{\lambda F^T F}{t D} \right) \right. \\
&\quad + \frac{1}{2} \frac{\lambda^2}{t^2} \left(\frac{F^T F}{D} z^1 - \frac{F^T}{\sqrt{D}} \omega \sqrt{t} \right)^T \left(I + \frac{\lambda F^T F}{t D} \right)^{-1} \left(\frac{F^T F}{D} z^1 - \frac{F^T}{\sqrt{D}} \omega \sqrt{t} \right) \\
&\quad \left. - \frac{\lambda}{2t} \left\| -\frac{F}{\sqrt{D}} z^1 + \omega \sqrt{t} \right\|^2 \right] \tag{53}
\end{aligned}$$

$$\begin{aligned}
&= \lim_{N \rightarrow \infty} \frac{1}{N} \mathbb{E}_{F, z^1, \omega} \left[-\frac{1}{2} \log \det \left(I + \frac{\lambda F^T F}{t D} \right) + \frac{\lambda^2}{2t^2} \left(\frac{F}{\sqrt{D}} z^1 \right)^T \frac{F}{\sqrt{D}} \left(I + \frac{\lambda F^T F}{t D} \right)^{-1} \frac{F^T}{\sqrt{D}} \left(\frac{F}{\sqrt{D}} z^1 \right) \right. \\
&\quad \left. - \frac{\lambda}{2t} \left\| -\frac{F}{\sqrt{D}} z^1 \right\|^2 + \frac{\lambda^2}{2t^2} \left(\frac{F^T}{\sqrt{D}} \omega \sqrt{t} \right)^T \left(I + \frac{\lambda F^T F}{t D} \right)^{-1} \left(\frac{F^T}{\sqrt{D}} \omega \sqrt{t} \right) - \frac{\lambda}{2t} \left\| \omega \sqrt{t} \right\|^2 \right] \tag{54}
\end{aligned}$$

Now with a rotation we can position in the basis of the eigenvectors of $\frac{F^T F}{N}$, with eigenvalues σ_k^2 .

$$= \lim_{N \rightarrow \infty} \frac{1}{N} \sum_i^N \left[-\frac{\lambda}{2} \right] + \frac{1}{N} \sum_k^D \left[-\frac{1}{2} \log \left(1 + \frac{\lambda}{\alpha_D t} \sigma_k^2 \right) + \frac{\lambda^2}{2\alpha_D^2 t^2} \left(\frac{\sigma_k^4}{1 + \frac{\lambda}{\alpha_D t} \sigma_k^2} \right) - \frac{\lambda}{2\alpha_D t} \sigma_k^2 + \frac{\lambda^2}{2\alpha_D t^2} \left(\frac{t\sigma_k^2}{1 + \frac{\lambda}{\alpha_D t} \sigma_k^2} \right) \right] \tag{55}$$

$$= -\frac{\lambda}{2} + \lim_{N \rightarrow \infty} \frac{1}{N} \sum_k \left[-\frac{1}{2} \log \left(1 + \frac{\lambda}{\alpha_D t} \sigma_k^2 \right) + \frac{\lambda^2}{2\alpha_D t} \left(\frac{\sigma_k^4}{\alpha_D t + \lambda \sigma_k^2} \right) - \frac{\lambda}{2\alpha_D t} \sigma_k^2 + \frac{\lambda^2}{2t} \left(\frac{t\sigma_k^2}{\alpha_D t + \lambda \sigma_k^2} \right) \right] \tag{56}$$

$$= -\frac{\lambda}{2} + \lim_{N \rightarrow \infty} \frac{1}{N} \sum_k \left[-\frac{1}{2} \log \left(1 + \frac{\lambda}{\alpha_D t} \sigma_k^2 \right) \right] \tag{57}$$

Here we have assumed that $\alpha_D < 1$. Taking the limit $N \rightarrow \infty$ the sum becomes an integration over the distribution ν of σ^2 , which is the bulk of a Marchenko-Pastur distribution

$$\zeta_t(\lambda) = -\frac{\lambda}{2} - \frac{\alpha_D}{2} \int \nu_{\alpha_D}(d\sigma^2) \log \left(1 + \frac{\lambda \sigma^2}{\alpha_D t} \right) \tag{58}$$

with

$$d\nu_\gamma(x) = \frac{1}{2\pi} \frac{\sqrt{(\gamma^+ - x)(\gamma^- - x)}}{\gamma x} \mathbb{I}(x \in [\gamma^-, \gamma^+]) \tag{59}$$

$$\gamma^\pm = (1 \pm \sqrt{\gamma})^2 \tag{60}$$

If we compute everything at $\lambda = 1$ this becomes

$$\zeta_t(1) = -\frac{1}{2} \int \nu_{\alpha_D}(d\sigma^2) \left[\log \left(1 + \frac{\sigma^2}{\alpha_D t} \right) \right] - \frac{1}{2} \tag{61}$$

Taking the derivative

$$\zeta'(\lambda) = -\frac{\alpha_D}{2} \int \nu_{\alpha_D}(d\sigma^2) \frac{\sigma^2}{\alpha_D t + \lambda \sigma^2} \tag{62}$$

$$\zeta'(1) = -\frac{1}{2} \tag{63}$$

We can also use replica theory, which will be necessary in the non-linear case, and compare the results. The replicated ζ reads

$$\mathbb{E} \mathcal{Z}^n = \mathbb{E}_{F, \omega} \mathbb{E}_{z^{0:n}} e^{-\frac{\lambda}{2t} \sum_{a'} \| \frac{F z^0}{\sqrt{D}} - \frac{F z^{a'}}{\sqrt{D}} \|^2 - \frac{\lambda \omega}{t} \sum_{a'} \left(\frac{F z^0}{\sqrt{D}} - \frac{F z^{a'}}{\sqrt{D}} \right) - \frac{\lambda}{2} \|\omega\|^2} \tag{64}$$

and with the same derivation shown in [B.2](#)

$$G_E = \int D\omega \int D\gamma \int Du^0 \log \left(\int Du e^{-\frac{\lambda}{2t} (u^0 - \sqrt{q_d - q_0} u - m u^0 + \sqrt{q_0 - m^2} \gamma)^2} - \frac{\lambda\omega}{\sqrt{t}} (u^0 - \sqrt{q_d - q_0} u - m u^0 + \sqrt{q_0 - m^2} \gamma) - \frac{\lambda}{2} \omega^2 \right) \quad (65)$$

$$\begin{aligned} &= \int D\omega \int D\gamma \int Du^0 \left[-\frac{\lambda}{2t} \left((1-m)u^0 + \sqrt{q_0 - m^2} \gamma \right)^2 - \frac{\lambda\omega}{\sqrt{t}} \left((1-m)u^0 + \sqrt{q_0 - m^2} \gamma \right) - \frac{\lambda}{2} \omega^2 \right. \\ &\quad \left. - \frac{1}{2} \log \left(1 + \frac{\lambda(q_d - q_0)}{t} \right) \right. \\ &\quad \left. + \frac{1}{2} \left(1 + \frac{\lambda(q_d - q_0)}{t} \right)^{-1} \left(\frac{\lambda}{t} \sqrt{q_d - q_0} \left((1-m)u^0 + \sqrt{q_0 - m^2} \gamma \right) + \frac{\lambda\omega}{t} \sqrt{q_d - q_0} \right)^2 \right] \end{aligned} \quad (66)$$

$$= -\frac{1}{2} \left(\lambda + \log \left(1 + \frac{\lambda(q_d - q_0)}{t} \right) + \frac{\lambda}{t} (1 - 2m + q_0) - \frac{\lambda^2 (q_d - q_0) (1 - 2m + q_0 + t)}{t^2 \left(1 + \frac{\lambda(q_d - q_0)}{t} \right)} \right) \quad (67)$$

The saddle point equations then become

$$\frac{\partial \zeta}{\partial \hat{q}_d} = 0 \quad q_d = \frac{1}{1 - \hat{q}_d + \hat{q}_0} + \frac{\hat{m}^2 + \hat{q}_0}{(1 - \hat{q}_d + \hat{q}_0)^2} \quad (68)$$

$$\frac{\partial \zeta}{\partial \hat{q}_0} = 0 \quad q_0 = \frac{1}{1 - \hat{q}_d + \hat{q}_0} + \frac{\hat{m}^2 + \hat{q}_d - 1}{(1 - \hat{q}_d + \hat{q}_0)^2} \quad (69)$$

$$\frac{\partial \zeta}{\partial \hat{m}} = 0 \quad m = \frac{\hat{m}}{1 - \hat{q}_d + \hat{q}_0} \quad (70)$$

$$\frac{\partial \zeta}{\partial q_d} = 0 \quad \hat{q}_d = \frac{2}{\alpha_D} \left(-\frac{1}{2} \right) \frac{\lambda (t + (-1 - 2m + q_0 + t)\lambda)}{(t + (q - q_0)\lambda)^2} \quad (71)$$

$$\frac{\partial \zeta}{\partial q_0} = 0 \quad \hat{q}_0 = -\frac{2}{\alpha_D} \left(-\frac{1}{2} \right) \frac{(1 - 2m + q_0 + t)\lambda^2}{(t + (q - q_0)\lambda)^2} \quad (72)$$

$$\frac{\partial \zeta}{\partial m} = 0 \quad \hat{m} = \frac{1}{\alpha_D} \left(-\frac{1}{2} \right) \left(-\frac{2\lambda}{t} + \frac{2(q - q_0)\lambda^2}{t^2 \left(1 + \frac{(q - q_0)\lambda}{t} \right)} \right). \quad (73)$$

Solving these saddle point equations we recover perfect agreement with [Eq. \(61\)](#).

B.2 Non-linear case

The replicated partition function reads

$$\mathbb{E} \mathcal{Z}^n = \mathbb{E}_{F, \omega} \mathbb{E}_{z^{0:n}} e^{-\frac{\lambda}{2t} \sum_{a'} \|\sigma\left(\frac{Fz^0}{\sqrt{D}}\right) - \sigma\left(\frac{Fz^{a'}}{\sqrt{D}}\right) + \omega \sqrt{t}\|^2} \quad (74)$$

$$= \mathbb{E}_{F, \omega} \mathbb{E}_{z^{0:n}} \int \frac{d\hat{u} du}{2\pi} e^{-\frac{\lambda}{2t} \sum_i \sum_{a'} (\sigma(u_i^0) - \sigma(u_i^{a'})) + \omega_i \sqrt{t})^2} e^{-i \sum_i \sum_{a=0}^n \hat{u}_i^a u_i^a + \sum_a \frac{i}{\sqrt{D}} \sum_{ik} \hat{u}_i^a F_{ik} z_k^a} \quad (75)$$

$$= \mathbb{E}_{\omega} \mathbb{E}_{z^{0:n}} \int \frac{d\hat{u} du}{2\pi} e^{-\frac{\lambda}{2t} \sum_i \sum_{a'} (\sigma(u_i^0) - \sigma(u_i^{a'}) + \omega_i \sqrt{t})^2} e^{-i \sum_i \sum_{a=0}^n \hat{u}_i^a u_i^a - \frac{1}{2D} \sum_{ik} (\sum_a \hat{u}_i^a z_k^a)^2} \quad (76)$$

$$= \mathbb{E}_{\omega} \mathbb{E}_{z^{0:n}} \int \frac{d\hat{u} du}{2\pi} e^{-\frac{\lambda}{2t} (1 + \frac{\lambda}{\Delta t}) \sum_i \sum_{a'} (\sigma(u_i^0) - \sigma(u_i^{a'}) + \omega_i \sqrt{t})^2} e^{-i \sum_i \sum_{a=0}^n \hat{u}_i^a u_i^a - \frac{1}{2D} \sum_{ab} (\sum_i \hat{u}_i^a \hat{u}_i^b) (\sum_k z_k^a z_k^b)} \quad (77)$$

$$= \int dq d\hat{q} e^{nN\phi_{\lambda}(q, \hat{q})} \quad (78)$$

with the overlaps defined as

$$q_{ab} = \frac{1}{D} \sum_k z_k^a z_k^b \quad (79)$$

so that we could write the replicated action

$$\zeta(q, \hat{q}) = -\frac{1}{2n} \frac{D}{N} \sum_{ab=0}^n q_{ab} \hat{q}_{ab} + \frac{D}{N} G_S(\hat{q}) + G_E(q) \quad (80)$$

with

$$G_S = \frac{1}{n} \log \mathbb{E}_{z^0:n} e^{\frac{1}{2} \sum_{ab} \hat{q}_{ab} z^a z^b} \quad (81)$$

$$G_E = \frac{1}{n} \log \int D\omega \int \prod_{a=0}^n \frac{d\hat{u}_a du_a}{2\pi} e^{-\frac{\lambda}{2t} \sum_{a'} (\sigma(u^0) - \sigma(u^{a'})) + \omega \sqrt{t} - i \sum_{a=0}^n \hat{u}^a u^a - \frac{1}{2} \sum_{ab} \hat{u}^a \hat{u}^b q_{ab}} \quad (82)$$

Using the replica symmetric Ansatz

$$q_{ab} = \begin{pmatrix} 1 & m & \dots & m \\ m & q_d & & q_0 \\ \vdots & & \ddots & \\ m & q_0 & & q_d \end{pmatrix}; \quad \hat{q}_{ab} = \begin{pmatrix} 0 & \hat{m} & \dots & \hat{m} \\ \hat{m} & \hat{q}_d & & \hat{q}_0 \\ \vdots & & \ddots & \\ \hat{m} & \hat{q}_0 & & \hat{q}_d \end{pmatrix} \quad (83)$$

we find

$$\zeta(q_d, q_0, m, \hat{q}_d, \hat{q}_0, \hat{m}) = -\alpha_D m \hat{m} - \frac{\alpha_D}{2} (q_d \hat{q}_d - q_0 \hat{q}_0) + \alpha_D G_S(\hat{q}_d, \hat{q}_0, \hat{m}) + G_E(q_d, q_0, m) \quad (84)$$

with

$$G_S(\hat{q}_d, \hat{q}_0, \hat{m}) = -\frac{1}{2} \log(1 - \hat{q}_d + \hat{q}_0) + \frac{1}{2} \frac{\hat{m}^2 + \hat{q}_0}{1 - \hat{q}_d + \hat{q}_0} \quad (85)$$

and for the energetic term

$$G_E = \frac{1}{n} \log \int D\omega \int \prod_{a=0}^n \frac{d\hat{u}_a du_a}{2\pi} e^{-\frac{\lambda}{2t} \sum_{a'} (\sigma(u^0) - \sigma(u^{a'}) + \omega\sqrt{t})^2 - i \sum_{a=0}^n \hat{u}^a u^a - \frac{1}{2} \sum_{ab} \hat{u}^a \hat{u}^b q_{ab}} \quad (86)$$

$$= \frac{1}{n} \log \int D\omega \int \frac{du^0 d\hat{u}^0}{2\pi} \prod_{a'=1}^n \frac{du^{a'} d\hat{u}^{a'}}{2\pi} e^{-\frac{\lambda}{2t} \sum_{a'} (\sigma(u^0) - \sigma(u^{a'}) + \omega\sqrt{t})^2} \\ \times e^{-\sum_{a'} i\hat{u}^{a'} u^{a'} - i\hat{u}^0 u^0 - \frac{1}{2} (\hat{u}^0)^2 - m\hat{u}^0 \sum_{a'} \hat{u}^{a'} - \frac{1}{2} (q_d - q_0) \sum_{a'} (\hat{u}^{a'})^2 - \frac{1}{2} q_0 (\sum_{a'} \hat{u}^{a'})^2} \quad (87)$$

$$= \frac{1}{n} \log \int D\omega \int \frac{du^0}{\sqrt{2\pi}} \prod_{a'=1}^n \frac{du^{a'} d\hat{u}^{a'}}{2\pi} e^{\frac{1}{2} (m \sum_{a'} \hat{u}^{a'} + iu^0)^2} e^{-\frac{\lambda}{2t} \sum_{a'} (\sigma(u^0) - \sigma(u^{a'}) + \omega\sqrt{t})^2} \\ \times e^{-\sum_{a'} i\hat{u}^{a'} u^{a'} - \frac{1}{2} (q_d - q_0) \sum_{a'} (\hat{u}^{a'})^2 - \frac{1}{2} q_0 (\sum_{a'} \hat{u}^{a'})^2} \quad (88)$$

$$= \frac{1}{n} \log \int D\omega \int D\gamma \int \frac{du^0}{\sqrt{2\pi}} e^{-\frac{1}{2} (u^0)^2} \int \prod_{a'=1}^n \frac{du^{a'} d\hat{u}^{a'}}{2\pi} e^{-\frac{\lambda}{2t} \sum_{a'} (\sigma(u^0) - \sigma(u^{a'}) + \omega\sqrt{t})^2} \\ \times e^{-i \sum_{a'} \hat{u}^{a'} (u^{a'} - mu^0 + \sqrt{q_0 - m^2} \gamma) - \frac{1}{2} (q_d - q_0) \sum_{a'} (\hat{u}^{a'})^2} \quad (89)$$

$$= \frac{1}{n} \log \int D\omega \int D\gamma \int Du^0 \left(\int \frac{du}{\sqrt{2\pi}} e^{-\frac{\lambda}{2t} (\sigma(u^0) - \sigma(u) + \omega\sqrt{t})^2} \frac{1}{\sqrt{q_d - q_0}} e^{-\frac{1}{2(q_d - q_0)} (u - mu^0 + \sqrt{q_0 - m^2} \gamma)^2} \right)^n \quad (90)$$

$$= \int D\omega \int D\gamma \int Du^0 \log \left(\int Du e^{-\frac{\lambda}{2t} (\sigma(u^0) - \sigma(\sqrt{q_d - q_0} u + mu^0 - \sqrt{q_0 - m^2} \gamma) + \sqrt{t}\omega)^2} \right). \quad (91)$$

We can then take derivatives to obtain the saddle point equations, which will of course depend on the choice of the non-linearity σ , and solve them numerically.

C Equivalence between Collapse and Condensation

In order to establish that the condensation and collapse phenomena happen at the same time, $t_c = t_{cond}$, we would therefore need to prove that

$$\zeta'_{t_c}(1) = -\frac{1}{2}. \quad (92)$$

We consider a typical data to be a diffused version of one of the starting training points

$$x_t = \xi^1 + \sqrt{t}\omega. \quad (93)$$

Notice that here we use the variance exploding diffusion process for homogeneity with the rest of the paper, but this analysis does not depend on the diffusion protocol, as long as we consider a typical point.

Write $\zeta(\lambda)$ as

$$\zeta(\lambda) = \mathbb{E}_{\xi^1} \mathbb{E}_{p(x_t|\xi^1)} \log \mathbb{E}_{\xi} p_{\lambda}(x_t|\xi) \quad (94)$$

where the data points come form a prior distribution, $\xi^1, \xi \sim p(\xi)$, and the likelihood has the form

$$p_{\lambda}(x_t|\xi) \propto e^{-\frac{\lambda}{2t} \|x_t - \xi\|^2}. \quad (95)$$

Then we compute $\zeta'(\lambda)$ taking the derivative

$$\partial_\lambda \log \mathbb{E}_\xi p_\lambda(x_t|\xi) = \frac{\int -\frac{\|x_t - \xi\|^2}{2t} p_\lambda(x_t|\xi) p(\xi) d\xi}{\int p_\lambda(x_t|\xi) p(\xi) d\xi} \quad (96)$$

$$= \int -\frac{\|x_t - \xi\|^2}{2t} p_\lambda(\xi|x_t) d\xi \quad (97)$$

so we can write this quantity as an average with respect to the posterior distribution $p(\xi|x_t)$, which we will indicate with $\langle \cdot \rangle_{\xi|x}$. Substituting $\lambda = 1$ and applying the Nishimori condition [26] we finally obtain

$$\zeta'(1) = \mathbb{E}_{\xi^1} \left[\mathbb{E}_{x|\xi^1} \left[\left\langle -\frac{\|x_t - \xi\|^2}{2t} \right\rangle_{\xi|x} \right] \right] \quad (98)$$

$$= \mathbb{E}_{\xi^1} \left[\mathbb{E}_{x|\xi^1} \left[-\frac{\|x_t - \xi^1\|^2}{2t} \right] \right] \quad (99)$$

$$= -\frac{1}{2}. \quad (100)$$

D Onset Time: Computation of the Generating function

D.1 Linear case

As explained in Section 2, we need to compute the cumulant generating function as

$$\zeta_t(\lambda) = \lim_{N \rightarrow \infty} \frac{1}{N} \mathbb{E}_{F, z^0} \log \mathbb{E}_z e^{-\frac{\lambda}{2t} \left\| \frac{Fz}{\sqrt{D}} - \frac{Fz^0}{\sqrt{D}} \right\|^2} \quad (101)$$

$$= \lim_{N \rightarrow \infty} \frac{1}{N} \mathbb{E}_{F, z^0} \log \int \frac{dz}{\sqrt{2\pi}} e^{-\frac{1}{2} z (I_D + \frac{\lambda}{t} \frac{F^T F}{D}) z + \frac{\lambda}{t} z (\frac{F^T F}{D} z^0) - \frac{\lambda}{2t} \left\| \frac{Fz^0}{\sqrt{D}} \right\|^2} \quad (102)$$

$$= \lim_{N \rightarrow \infty} \frac{1}{N} \mathbb{E}_{F, z^0} \left[-\frac{1}{2} \log \det \left(I_D + \frac{\lambda}{t} \frac{F^T F}{D} \right) + \frac{1}{2} \frac{\lambda^2}{t^2} \left(\frac{F^T F}{D} z^0 \right)^T \left(I_D + \frac{\lambda}{t} \frac{F^T F}{D} \right)^{-1} \left(\frac{F^T F}{D} z^0 \right) - \frac{\lambda}{2t} \left\| \frac{Fz^0}{\sqrt{D}} \right\|^2 \right]. \quad (103)$$

Now with a rotation we can position in the basis of the eigenvectors of $\frac{F^T F}{N}$, with eigenvalues σ_k^2

$$= \lim_{N \rightarrow \infty} \frac{1}{N} \sum_k^D \left[-\frac{1}{2} \log \left(1 + \frac{\lambda}{\alpha_D t} \sigma_k^2 \right) + \frac{\lambda^2}{2\alpha_D^2 t^2} \left(\frac{\sigma_k^4}{1 + \frac{\lambda}{\alpha_D t} \sigma_k^2} \right) - \frac{\lambda}{2\alpha_D t} \sigma_k^2 \right] \quad (104)$$

$$= \lim_{N \rightarrow \infty} \frac{1}{N} \sum_k \left[-\frac{1}{2} \log \left(1 + \frac{\lambda}{\alpha_D t} \sigma_k^2 \right) - \frac{\lambda}{2} \frac{\sigma_k^2}{\alpha_D t + \lambda \sigma_k^2} \right]. \quad (105)$$

Here we have assumed that $\alpha_D < 1$. Replacing with the law ν for the bulk of the Marchenko-Pastur distribution we have

$$\zeta_t(\lambda) = -\frac{\alpha_D}{2} \int \nu_{\alpha_D}(d\sigma^2) \left[\log \left(1 + \frac{\lambda \sigma^2}{\alpha_D t} \right) + \frac{\lambda \sigma^2}{\alpha_D t + \lambda \sigma^2} \right]. \quad (106)$$

This expression of ζ at $\lambda = 1$ is then used to obtain $\phi(\alpha, t)$.

D.2 Non-linear case

In case of non-linear functions that define the manifold, we are going to employ the replica method to compute the REM free-energy, as we performed for the condensation time. First we need to compute the cumulant generating function as

$$\zeta_t(\lambda) = \lim_{N \rightarrow \infty} \frac{1}{N} \mathbb{E}_x \log \mathbb{E}_\xi [e^{-\frac{\lambda}{2t} \|x - \xi\|^2}] \quad (107)$$

$$= \lim_{N \rightarrow \infty} \frac{1}{N} \mathbb{E}_{F, z_0} \log \mathbb{E}_z [e^{-\frac{\lambda}{2t} \|\sigma(\frac{Fz_0}{\sqrt{D}}) - \sigma(\frac{Fz}{\sqrt{D}})\|^2}] \quad (108)$$

$$= \lim_{N \rightarrow \infty} \frac{1}{N} \mathbb{E}_{F, z_a} [e^{-\frac{\lambda}{2t} \sum_{a'} \|\sigma(\frac{Fz_0}{\sqrt{D}}) - \sigma(\frac{Fz_{a'}}{\sqrt{D}})\|^2}]. \quad (109)$$

Using the replica symmetric ansatz we obtain

$$\zeta_t(q_d, q_0, m, \hat{q}_d, \hat{q}_0, \hat{m}) = -\alpha_D m \hat{m} - \frac{\alpha_D}{2} (q_d \hat{q}_d - q_0 \hat{q}_0) + \alpha_D G_S(\hat{q}_d, \hat{q}_0, \hat{m}) + G_E(q_d, q_0, m) \quad (110)$$

with

$$G_S(\hat{q}_d, \hat{q}_0, \hat{m}) = -\frac{1}{2} \log(1 - \hat{q}_d + \hat{q}_0) + \frac{1}{2} \frac{\hat{m}^2 + \hat{q}_0}{1 - \hat{q}_d + \hat{q}_0} \quad (111)$$

and for the energetic term

$$G_E(q_d, q_0, m) = \int D\gamma \int Du^0 \log \left(\int Du e^{-\frac{\lambda}{2t} (\sigma(u^0) - \sigma(\sqrt{q_d - q_0}u + mu^0 - \sqrt{q_0 - m^2}\gamma))^2} \right). \quad (112)$$

Then one can solve the saddle point equation, which will depend on the choice of the non-linearity σ , and obtain ζ at the fixed point.

E Computation of the KL-Divergence

The Kullback-Leibler (KL) divergence is a type of statistical distance between two probability density functions. Given the two distributions $p_0(x)$, namely the ground-truth distribution of the data, and $p_{t, \mathcal{D}}^{emp}(x)$, namely the empirical distribution of the data according to the model, the full KL divergence between these two functions assumes the following expression

$$\lim_{N \rightarrow \infty} \frac{1}{N} \mathbb{E}_{\mathcal{D}} D_{KL} [p_0 | p_{t, \mathcal{D}}^{emp}] = \lim_{N \rightarrow \infty} \frac{1}{N} \mathbb{E}_{\mathcal{D}} \left[\int dx p_0(x) \log p_0(x) - \int dx p_0(x) \log p_{t, \mathcal{D}}(x) \right] \quad (113)$$

$$= -s_0 + \tilde{D}_{KL} [p_0 | p_t^{emp}], \quad (114)$$

where s_0 is the entropy of the p_0 distribution and \tilde{D}_{KL} is the only time-dependent component of the KL divergence. Since we are studying a data-model where $p_0(x)$ is defined on a support having a lower dimensionality with respect to the N -dimensional data-space, we expect the entropy s_0 to diverge. This issue might be controlled by adding some noise to either the latent data points z^μ or the features in F , but we will not engage into this analysis. Nevertheless, for studying the dependence on t we can compute the \tilde{D}_{KL} function in order to find the *generalization time* t_g at which the distance between the two distribution is minimal. We derive below \tilde{D}_{KL} in both the linear and

non-linear manifold cases by expressing this quantity in terms of time-dependent free-energy function in the REM formalism.

The time-dependent part of the KL divergence is given by

$$\tilde{D}_{KL}[p_0|p_t^{emp}] = - \lim_{N \rightarrow \infty} \frac{1}{N} \mathbb{E}_{\mathcal{D}} \int dx p_0(x) \log p_{t,\mathcal{D}}^{emp}(x), \quad (115)$$

with $x \sim \sigma(\frac{Fz}{\sqrt{D}})$, $z \sim \mathcal{N}(0, I_D)$, $F \in \mathbb{R}^{N \times D}$, and the empirical score reads

$$\log p_{t,\mathcal{D}}^{emp}(x) = \log \frac{1}{P\sqrt{2\pi t}^N} \sum_{\mu=1}^P e^{-\frac{1}{2t} \|x - \xi^\mu\|^2} \simeq N \left[\Phi_t(x) - \alpha - \frac{1}{2} \log(2\pi t) \right], \quad (116)$$

where

$$\Phi_t(x) = \frac{1}{N} \log \sum_{\mu=1}^P e^{-\frac{1}{2t} \|x - \xi^\mu\|^2} \quad (117)$$

is again minus the free energy density of a REM. For $P, N \rightarrow \infty$ with $\alpha = \log P/N$ this concentrates to

$$\phi(\alpha, t) = \lim_{N \rightarrow \infty} \mathbb{E}_{x \sim p_0} [\Phi_t(x)], \quad (118)$$

and to know this limit we need to compute the large deviation function.

E.1 Linear case

In case of a linear manifold we can compute \tilde{D}_{KL} in terms of the free-energy of a REM, as in Eq. (36). The computation of the free-energy function coincides with the one performed in Appendix D.1.

E.2 Non-linear case

In case of non-linear functions that define the manifold, we are going to employ the replica method to compute the REM free-energy, as we performed for the condensation time. The computation coincides with the one performed in Appendix D.2.